Journal for ImmunoTherapy of Cancer

Integrating interferon gamma receptor pathways, antigenicity, and immune contexture as predictors of immunotherapeutic strategies for mucosal melanomas

Matilde Monti,[1] Sara Picinoli,[1] Anna Bozzola,[2] Marco Ferrari,[3,4] Mattia Bugatti,[1,2] Irene Pezzali,[1] Marco Carlomagno,[5] Giada Carta,[5] Matteo Orlandi,[5] Giacomo Lora,[5] Luisa Benerini Gatta,[6] Francesco Missale,[7] Giorgia Ferrari,[1] Valentina Baldazzi,[1] Sara Rezzola,[1] Giovanna Tabellini,[1] Silvia Parolini,[1,8,9] Marcello Manfredi,[10,11] Veronica De Giorgis,[10,11] Emilio Marengo,[12] Mario Turri-Zanoni,[13] Piero Nicolai,[3,4] Francesca Consoli,[14] Davide Lombardi,[15] Paolo Martini,[1] Jinglun Li,[16] Obi Griffith,[17] Malachi Griffith,[17] Marzia Rossato,[5] William Vermi [1,18]

To cite: Monti M, Picinoli S, Bozzola A, *et al*. Integrating interferon gamma receptor pathways, antigenicity, and immune contexture as predictors of immunotherapeutic strategies for mucosal melanomas. *Journal for ImmunoTherapy of Cancer* 2026;**14**:e012222. doi:10.1136/jitc-2025-012222

► Additional supplemental material is published online only. To view, please visit the journal online (https://doi.org/10.1136/jitc-2025-012222).

Accepted 18 January 2026

For numbered affiliations see end of article.

Correspondence to
Professor William Vermi;
william.vermi@unibs.it

ABSTRACT

Background Mucosal melanomas (MM) arise from mucosal melanocytes at various anatomical sites. These tumors are rare, highly aggressive, and often associated with poor outcomes. Current treatments, including immune checkpoint inhibitors, show limited efficacy in advanced disease. Compared with cutaneous melanomas, there is a lack of data on the immunogenicity and interferon (IFN)-γ sensitivity of MM. In this study, we examined these features in sino-nasal melanomas (SN-MM) cell lines and clinical samples using microscopy and functional genomics.

Methods The immune contexture of SN-MM was analyzed by immunohistochemistry on 48 tumor biopsies. RNA sequencing and mass spectrometry-based proteomic approaches were used to study the IFN-γ receptor (IFNGR) pathways in five patient-derived SN-MM cell lines. Moreover, their IFN-γ sensitivity, in terms of cell viability, IFNGR/JAK/STAT signaling pathway and IFN-γ inducible proteins, was evaluated by flow cytometry and immunoblots. Neoantigen prediction was performed through integrated whole exome sequencing and RNA-sequencing analysis using pVAC-Seq. Immune effector functions were evaluated in co-culture in vitro assays.

Results SN-MM tumors are mainly immune "desert" with few tumor-infiltrating lymphocytes and contain immunosuppressive macrophages, features linked to poor prognosis; moreover, tumor cells are largely CD274/programmed death-ligand 1 negative. SN-MM cell lines express transcripts for melanocytic and cancer testis antigens; moreover, sequencing analysis identified a repertoire of high-confidence neoantigens, including candidates derived from recurrently mutated oncogenic drivers. Functional assays revealed that SN-MM cells are susceptible to NK cell-mediated killing. In terms of IFN-γ sensitivity, SN-MM cells show normal surface expression of IFNGR and maintain the integrity of the IFNGR/JAK/STAT signaling pathway. Transcriptomic and proteomic analyses demonstrate that SN-MM cell lines, as a group, respond to IFN-γ by upregulating genes involved in immune recognition and antigen presentation. In 60% of SN-MM lines, IFN-γ also induces cytotoxic and anti-proliferative effects, the release of CXCL10 and upregulation of CD274/PD-L1. The remaining SN-MM cell lines, characterized by poor differentiation, show refractoriness to these effects.

Conclusions SN-MM displays an immune-desert phenotype yet retains intrinsic immunogenicity. Most tumors preserve functional IFN-γ signaling, while poorly

WHAT IS ALREADY KNOWN ON THIS TOPIC

⇒ Immune checkpoint inhibitors (ICI) showed limited efficacy in advanced mucosal melanoma (MM), partially explained by low tumor mutational burden, scarce immunogenicity, and poor immune infiltration. This study is needed to explore the interferon (IFN)-γ sensitivity and immunogenicity of MM to predict immunotherapy response.

WHAT THIS STUDY ADDS

⇒ By using unique patient-derived sino-nasal melanomas (SN-MM) cell lines, we could prove their antigenicity along with a heterogeneous response to IFN-γ. Specifically, the IFN-γ-inducible programmed death-ligand 1 expression, release of CXCL10, and cytotoxicity were differentially regulated among SN-MM cell lines. Our findings suggested a combination of immune escape mechanisms leading to immune exclusion in MM tissues.

HOW THIS STUDY MIGHT AFFECT RESEARCH, PRACTICE OR POLICY

⇒ Combining immune contexture analysis with functional assays and neoantigen profiling could guide patient selection for immune therapy strategies.

differentiated cells show resistance to IFN-γ-mediated effects. These findings underscore heterogeneity in immune responsiveness and support functional immune profiling to refine immunotherapy strategies in MM.

INTRODUCTION

Advances in understanding the immune contexture and genomic landscape of cutaneous melanomas (CMs) have expanded treatment options for advanced disease.[1] However, these successes have not translated to non-skin melanomas, such as mucosal melanoma (MM), which remain highly aggressive and associated with poor clinical outcomes.[2 3] The head and neck region, including the nasal cavity and paranasal sinuses, represents the most common anatomical location of MM.[4] MM outcome is very poor, and the reasons behind this aggressive clinical behavior are only partially understood.[5 6] In addition, there is still no definitive consensus on the optimal management of MMs, particularly on the role of adjuvant treatments for loco-regional and systemic control.[5] BRAF V600 mutations are found in a negligible percentage of MMs[6 7] and systemic chemotherapies have demonstrated little or no survival benefit, with most patients early dying after the diagnosis for systemic dissemination. Moreover, the outcome of immune checkpoint inhibitors (ICI) treatment in patients with MM is controversial, suggesting that additional prospective clinical studies with larger scale populations are needed. Despite some advances in immunotherapeutic approaches for patients with advanced MM,[2 8] clinical studies suggest that these patients are, as a group, less responsive to ICI than those with CM.[3 9] The difference in response to ICI might partially be explained by their intrinsic level of immunogenicity[10] and immune contexture. As compared with CMs, MMs have a significantly lower tumor mutational burden, which might result in a reduced neoantigen load and tumor-infiltrating lymphocytes (TILs) density.[7 11] However, at variance with CM, MM immunogenicity and corresponding immune escape mechanisms are poorly understood.[11]

Cancers frequently harbor genomic and phenotypic alterations affecting genes involved in interferon (IFN) signaling pathways, which underline their heterogeneous responsiveness to IFN stimuli. IFN-γ plays a central role in antitumor immune responses, tumor immunogenicity, and the process of cancer immunoediting. Conversely, loss or attenuation of IFN-γ responsiveness confers a survival advantage to cancer cells by enabling immune evasion.[12 13] Specifically, the endogenously produced IFN-γ has a key role in immune surveillance modulating tumor cell immunogenicity and immune contexture. However, loss of the capacity to signal through the IFN-γ receptor (IFNGR) due to identifiable defects in the IFN-γ signaling cascade is well documented in human cancers.[14] IFN-γ induces reorganization of the IFNGR subunits, signaling via JAK/STAT,[15] resulting in the activation of interferon-stimulated response elements and gamma IFN activation sites within the promoters of IFN-γ-inducible genes. IFN-γ regulates cell cycle, antigen presentation, T-cell attracting chemokines, as well as promotes the expression of the inhibitory receptors programmed cell death ligand 1 (CD274/PD-L1), programmed cell death ligand 2 (CD273/PD-L2), cytotoxic T-lymphocyte associated protein 4,[16 17] and the immunosuppressive metabolite indoleamine 2,3-dioxygenase (IDO).[18] IFN-γ modulates tumor immunogenicity through induction of the major histocompatibility complex (MHC) class I and class II pathway of antigen processing and presentation in tumor cells for their recognition by $CD8^+$ and $CD4^+$ T cells, respectively, which are both required for an effective response to ICI.[19] The unresponsiveness to IFN-γ is one of the main cancer immune escape mechanisms along with the loss of MHC-I antigen presentation machinery, a feature predicting worse prognosis and resistance to immunotherapies.[12 19–22]

Recently, we developed five novel sino-nasal melanoma (SN-MM) cell lines that provide a unique model to study the immunobiology of MM.[23] These cell lines retain melanocytic identity, exhibit varying degrees of differentiation, and display tumorigenic potential both in vitro and in vivo. Using these systems and clinical samples, we investigated the MM immunogenicity and responsiveness to IFN-γ. Our results show that SN-MM cell lines express a rich repertoire of tumor neoantigens and maintain intact IFNGR/JAK/STAT signaling consistent with the transcriptomic and proteomic response to IFN-γ. While 60% of the cell lines were responsive in terms of cytotoxicity, cell growth inhibition, and PD-L1 expression, most clinical samples showed immune exclusion with a lack of CD274/PD-L1 expression. These findings suggest that a better understanding of MM's immune escape mechanisms, particularly related to IFN-γ, could guide more personalized immune therapy strategies. Functional assays measuring IFN-γ sensitivity could play a crucial role in patient selection for immune treatments.

MATERIAL AND METHODS

Human tissue samples

All human tissues and clinical information were obtained in compliance with the bioethical requirements, as detailed in online supplemental M&M. The study involved formalin-fixed paraffin-embedded (FFPE) biopsies obtained from 48 patients with clinical and pathology annotated SN-MM. Patients included in this study received surgery with curative or palliative intent. SN-MM was diagnosed and staged according to the available version of the WHO Classification of Head and Neck Tumors and the AJCC (American Joint Committee on Cancer) staging system, respectively.[24] Detailed characteristics of patients are shown in online supplemental table S1. Additional information on clinicopathological characteristics of patients and FFPE samples collection is reported in online supplemental M&M. The control group consisted of patients presenting malignant CM previously reported by our group.[25]

Histology and immunohistochemistry

FFPE tumor biopsies and cell-block sections were used for histology and immunohistochemistry (IHC). Histologic evaluation of H&E or IHC-stained sections of tumor samples and cell blocks was performed by two expert pathologists. IHC staining and RNAscope are detailed in online supplemental M&M. Primary antibodies used are listed in online supplemental table S2. Stained sections were evaluated using a digital microscopy approach and the immune markers were expressed as percentage of positive cells within the total amount of CD45-positive leukocytes, using a four-tiered scoring system, as described in online supplemental M&M.

Cell lines

Five human SN-MM cell lines, designated as SN-MM one to five, previously generated from tumor biopsies and extensively characterized by our group[23] were used in this study. Human A2058 and FO1 CM cell lines were used as control. Melanoma cell lines were cultured as described in online supplemental M&M. SN-MM cells were treated with 100 ng/mL of recombinant human IFN-γ (PeproTech, Rocky Hill, USA). Detailed information for the use of the IFN-γ for each experiment is described in online supplemental M&M.

In vitro co-culture assays

Peripheral blood mononuclear cells (PBMCs) were isolated from healthy donors. PBMCs were cultured in complete RPMI (Roswell Park Memorial Institute) medium supplemented with 100 U/mL rh-IL-2. T cells were activated with anti-CD3/anti-CD28 antibodies. PBMCs were co-incubated with tumor cells at different effector-to-target ratios, as detailed in online supplemental M&M. Anti-CD107a-PE was added to measure natural killer (NK) cell and $CD8^+$ T-cell degranulation. Tumor cells viability was evaluated by propidium iodide staining as described in online supplemental M&M.

Flow cytometry

The detailed methods are described in online supplemental M&M. In brief, the percentage of positive cells and median of fluorescence intensity (MFI) for Human Leukocyte Antigens (HLA)-ABC, HLA-DR, CD274/PD-L1, and IFNGR1 (online supplemental table S2) were evaluated on live cells. Cell viability was evaluated using the Pacific Blue Annexin V/SYTOX AADvanced Apoptosis Kit (Thermo Fisher Scientific). Samples were processed on MACS Quant Analyzer 16 (Miltenyi Biotec). Results were analyzed by FlowJo X software (TreeStar, Wilmington, North Carolina, USA).

The percentage of $CD107a^+$ cells was measured on $CD56^+$ NK cells and $CD8^+$ T cells. Propidium Iodide (PI) positive cells were measured on tumor cells identified based on forward and side scatter. Samples were processed on FACSCanto (Becton Dickinson, Mountain View, California, USA). Data were analyzed using the Diva software (Becton Dickinson).

Proteomic analysis

Sample proteins were digested and analyzed as described in online supplemental M&M. Statistical analysis was performed with MarkerView for the t-test (p value <0.05 and fold change >1.3) and MetaboAnalyst V.5.0 (www.metaboanalyst.org). Bioinformatic analysis was carried out using Ingenuity Pathways Analysis (IPA) software (Qiagen) and R V.4.4.1 (R Foundation for Statistical Computing, Vienna, Austria).

RNA sequencing

RNA sequencing (RNA-seq) libraries were prepared using the TruSeq RNA Sample Prep Kit V.2 (Illumina, San Diego, California, USA) and sequenced on NovaSeq6000 (Illumina) generating ~33 million 150 PE (phycoerythrin) reads per sample. After adapter trimming, reads were aligned to the *Homo sapiens* reference genome (Ensembl V.109) using STAR (V.2.7.9a). RSEM (RNA-Seq by Expectation-Maximization) was used for expression counting and TPM (transcripts per million) calculation (V.1.3.3). Differential expression analysis was performed with DESeq2 (V.1.30.1) with the apelglm method for log2-fold change (LFC) shrinkage. Expression data (log2(TPM+1)) of DepMap cell lines were downloaded from the DepMap portal (DepMap Public 24Q4, *https://depmap.org/portal/data_page/?tab=currentRelease*). Gene Set Enrichment Analysis (GSEA) (https://www.gsea-msigdb.org/gsea/downloads.jsp) was performed on genes pre-ranked according to LFC[26 27] using the Hallmarks gene set from MsigDB V.7.5 database (https://www.gsea-msigdb.org/gsea/msigdb). Gene Ontology (GO) enrichment analysis has been performed using clusterProfiler (V.3.18.1) with the function "simplify 0.7" applied. Single nucleotide variants (SNVs) of each cell line have been independently identified from resting and IFN-γ-treated conditions on pooled RNA-seq replicates (~100 M fragments each). Variants were identified based on the GATK Best Practice workflow using GATK HaplotypeCaller V.4.1.9.0. Subsequently, variants were annotated and ranked by putative pathogenicity using the CTAT-mutation pipeline (V.4.0.0). We retained only SNVs showing low population frequency (gnomad Allele Frequency (AF) <0.01) and predicted pathogenic, namely CHASM (p value <0.05) or VEST (p value <0.05), or pathogenic in COSMIC or in ClinVar.

In silico neoantigens prediction analysis

Human leukocyte antigen (HLA) typing was performed on five SN-MM cell lines by using Optitype, HLAHD and PHLAT algorithms as described in online supplemental M&M. The HLA types used for neoantigen predictions are reported in online supplemental table S3. Class I and class II neoantigen analysis was performed using pVACtools pVAC-Seq (V.6.0.0) for all non-synonymous variants in one or more transcripts against all class I and II alleles of each tumor for the HLA genes: HLA-A, HLA-B, HLA-C, DPA1/DPB1, DQA1/DQB1, DRBA/DRB1, DRB2, DRB3,

DRB5. A "pass" tier peptide was defined as detailed in online supplemental M&M.

Statistical analysis

The detailed methods are described in online supplemental M&M. In brief, the Mann-Whitney U test, Kruskal-Wallis test or Spearman's correlation test were used to analyze the association between immune cell densities and clinicopathological characteristics. Survival analysis was performed considering the overall survival (OS) as primary outcome and progression-free survival (PFS) as a secondary outcome. Cox proportional-hazards model, Kaplan-Meier method, and log-rank test were used to test the immune cell densities in univariate survival analysis. Immune contexture biomarkers showing association with OS with p<0.05 were included in a multivariable Cox proportional-hazards model to estimate the multivariable-adjusted HRs. Statistical analyses of the patients' series were performed using RStudio (Vienna, Austria).

Statistical significance for in vitro experiments was determined by applying two-way analysis of variance followed by Bonferroni post-test for multiple comparison. For all statistical tests, the level of significance was set at 0.05. Statistical analyses were performed using RStudio (Vienna, Austria) and GraphPad Prism Software (GraphPad Software, La Jolla, California, USA).

Additional methods

Detailed information on IHC, RNAscope, digital microscopy and image analysis, cell culture and co-culture experiments, MTS (3-(4,5-dimethylthiazol-2-yl)-5-(3-carboxymethoxyphenyl)-2-(4-sulfophenyl)-2H-tetrazolium, inner salt) assay, flow cytometry, western blots, mass spectrometry, ELISA, RNA-seq, bioinformatics and statistical analysis are included in the online supplemental M&M. Immunoscore classification is described in online supplemental figure S1. Patients' follow-up is reported in online supplemental table S1. Detailed information on the primary antibodies used is described in online supplemental table S2. The HLA types used for neoantigen predictions are reported in online supplemental table S3.

RESULTS

A desert immune contexture with myeloid cells predicts SN-MM unfavorable prognosis

The distribution pattern of immune cells in solid tumors is commonly classified into three phenotypes, namely "immune inflamed" characterized by lymphocytic infiltration within the tumor mass with the immune cells positioned in proximity to the tumor cells, "immune desert" typically lacking lymphocytes in either the tumor mass or at the periphery, although myeloid cells may be present, and "immune excluded" characterized by immune cells confined to the stroma surrounding tumor cell nests.[28] We tested the immune contexture of a cohort of 48 SN-MM cases by IHC. The cohort details are reported in online supplemental table S1. We performed immune cell mapping by testing the occurrence of $CD45^+$ tumor-infiltrating leukocytes (TILe), $CD3^+$ TILs, $CD8^+$ cytotoxic T lymphocytes (CTL), $CD20^+$ B lymphocytes, $CD163^+$ tumor-associated macrophages (TAM), $CD66^+$ neutrophils, $CD56^+$ NK cells and $CD303^+$ plasmacytoid dendritic cells (pDC) (figure 1A,B). First, we applied a digital microscopy approach to quantify the $CD45^+$ TILe and $CD8^+$ T cells. Density of $CD45^+$ TILe (mean±SEM: SN-MM 297.0±49.87 vs CM 1758±137.5; p<0.0001) and of $CD8^+$ T cells (mean±SEM: SN-MM 127.5±27.63 vs CM 397.9±85.28; p=0.0038) resulted significantly lower in SN-MM compared with CM (figure 1C,D). For the remaining immune cell populations, data are expressed as $CD45^+$ immune cell fractions and summarized in online supplemental table S4. Most SN-MM cases were immune desert (figure 1A), whereas a minor fraction of SN-MM displayed a higher density of $CD8^+$ CTL, $CD163^+$ TAM, and $CD20^+$ B cells (figure 1B); $CD66b^+$ neutrophils were also detectable, whereas $CD56^+$ NK and $CD303^+$ pDC were absent (figure 1 and online supplemental table S4). Of note, the fraction of triggering receptor expressed on myeloid cells 2 (TREM2)-expressing $CD163^+$ TAM was significantly higher in SN-MM cases with a poor $CD8^+$ CTL density as compared with $CD8^+$ CTL rich cases (mean±SEM: CD8 poor 432.3±81.1 vs CD8 rich 46.4±26.3; p=0.0008; figure 1E). Moreover, linear regression analysis proved that the high density of TREM2 is related to a poor CD8 density in SN-MM (p=0.03; figure 1F). We have recently shown that a fraction of TAM across human cancers express TREM2 and are immunosuppressive.[29] By RNAscope analysis of a set of SN-MM cases, we further revealed the expression of transforming growth factor-β by immunosuppressive $TREM2^+$ TAM (figure 1G,H). Finally, SN-MM cases were mainly negative for PD-L1 expression evaluated on the tumor cell fraction [tumor proportion score (TPS); online supplemental table S4]. These findings indicate that SN-MM are non-inflamed melanomas with a subgroup enriched in immunosuppressive myeloid cells.

By gene signatures and tissue cell mapping, the immune contexture has been considered a relevant prognosticator in various cancer types.[30] We tested and verified this hypothesis on the SN-MM retrospective cohort. Based on single-population density and combined immunoscore, SN-MM samples were divided into subgroups, as described in the online supplemental M&M, and survival analysis was performed. CD56 and CD303 biomarkers were excluded from the survival analysis since positive cases were almost absent (online supplemental table S4). Notably, low $CD45^+$ (≤199.9 cell/mm^2) and low $CD8^+$ (≤28.5 cell/mm^2) cell densities were associated with worse OS ($CD45^+$ p=0.0028; $CD8^+$ p=0.0014; figure 1I,J). High CD163 expression (score 2–3) was associated with shorter OS (p=0.035; figure 1K), whereas the expression of CD3 (p=0.3), CD20 (p=0.77) and CD66b (p=0.37) were not significantly associated with OS (figure 1L–N). The immunoscore predicted both OS (p=0.004) and PFS (p=0.018) at univariate analysis (figure 1O,P);

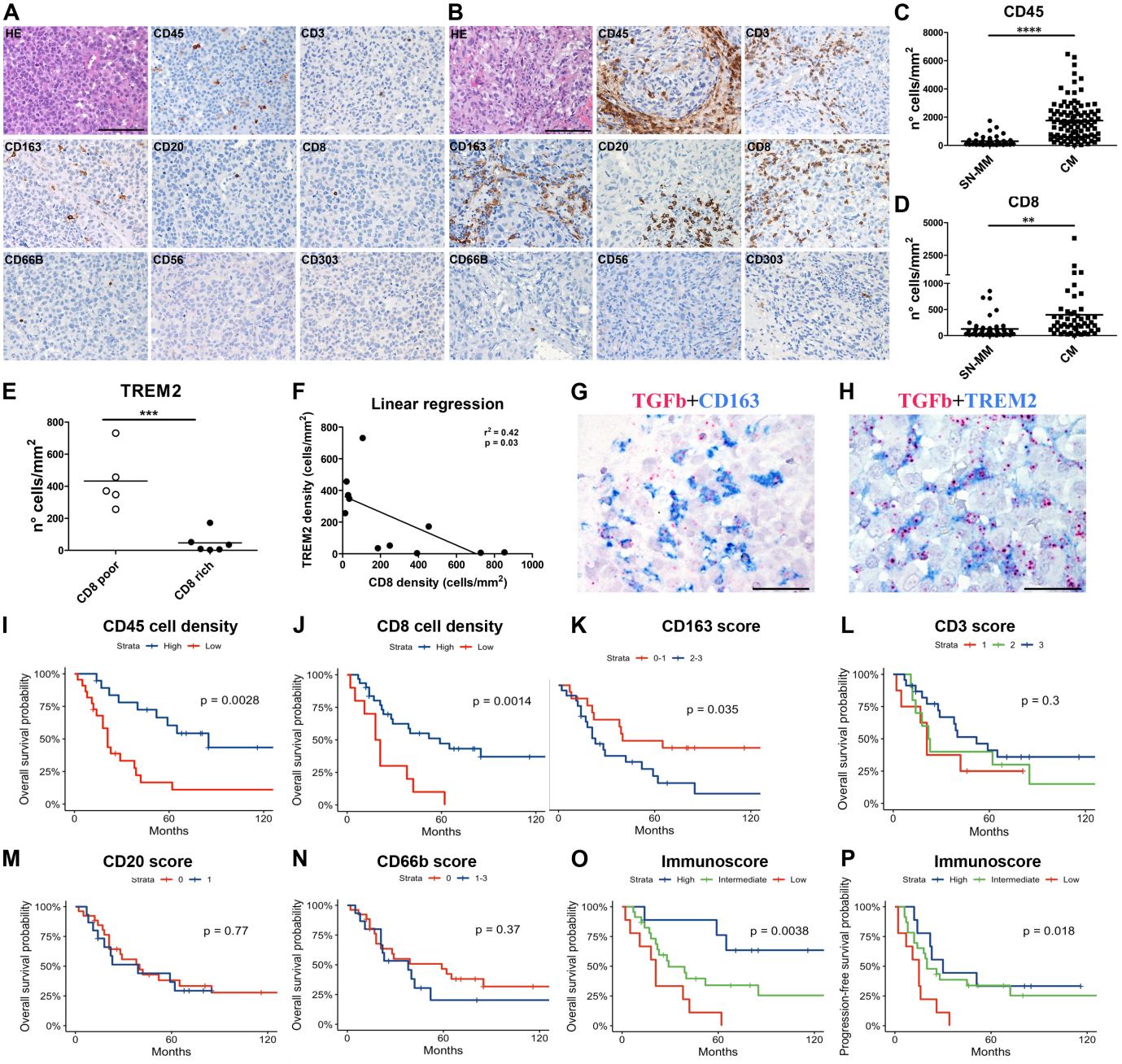

Figure 1 SN-MM are non-inflamed melanomas, and low immunoscore predicts poor prognosis. Representative cases of SN-MM lacking immune cell infiltrate (A) or displaying poor immune cells surrounding the tumor nests (B), stained as labeled. Magnification 200×; scale bar 100 µm. Scatter plots illustrate the distribution of CD45$^+$ leukocytes (C) and CD8$^+$ CTL (D) in SN-MM (n=48) and CM (n=101). A scatter plot illustrates the distribution of TREM2$^+$ TAMs (E) in CD8-poor (n=5) versus CD8-rich (n=6) SN-MM. The threshold for defining CD8-rich or CD8-poor SN-MM cases was defined based on the mean CD8$^+$ CTL density across the entire SN-MM cohort (n=48; mean±SEM: 127.5±27.6 cells/mm^2). Bars represent the mean values. The statistical significance was calculated by a Student's t-test. *p<0.05; ***p<0.001; ****p<0.0001. (F) Linear regression analysis between TREM2 density and CD8 density in SN-MM. (G–H) Representative images of TGF-β RNAscope in SN-MM cases, stained as labeled. Magnification 400×; scale bar 100 µm. (I–N) Kaplan-Meier plots showing the OS depending on the density of CD45$^+$ TILe (I) or CD8$^+$ CTL (J) or on the score of CD163$^+$ (K), CD3$^+$ (L), CD20$^+$ (M), and CD66b$^+$ (N). (O–P) Kaplan-Meier plots showing the OS (O) and PFS (P) probability of patients with SN-MM depending on the immunoscore level. For each SN-MM case, the immunoscore was calculated by summing the scores related to CD163, CD45, and CD8 categories and is classified as low (0–1), intermediate (2–3), or high (4–5). Immunoscore points equal to 2 are assigned to the categories of high CD45$^+$ and high CD8$^+$ cell density, immunoscore point equal to 1 is assigned to the category of CD163 low (0–1 score). CM, cutaneous melanomas; CTL, cytotoxic T lymphocytes; OS, overall survival; PFS, progression-free survival; SN-MM, sino-nasal melanoma; TGF, transforming growth factor; TILe, tumor-infiltrating leukocytes; TREM2, triggering receptor expressed on myeloid cells 2.

Table 1 Multivariable survival analysis on cM0 patients who received non-R^2 surgery (n=41)

	Overall survival		Progression-free survival	
Covariate	Cat., HR (95% CI)	P value	Cat., HR (95% CI)	P value
Immunoscore	High, REF Intermediate, 1.76 (0.43 to 7.27) Low, 8.11 (1.94 to 33.88)	0.43 **0.004**	High, REF Intermediate, 1.42 (0.44 to 4.56) Low, 3.42 (1.05 to 11.18)	0.56 **0.04**
Gender	Female, REF Male, 1.97 (0.79 to 4.88)	0.14	Female, REF Male, 1.06 (0.44 to 2.52)	0.90
Age (years)	1.00 (0.96 to 1.04)	0.91	0.99 (0.97 to 1.02)	0.64
T	3, REF 4a, 1.14 (0.38 to 3.38) 4b, 0.50 (0.14 to 1.76)	0.81 0.28	3, REF 4a, 0.92 (0.36 to 2.39) 4b, 1.17 (0.39 to 3.54)	0.87 0.78
Site	Nasal, REF Paranasal, 1.64 (0.63 to 4.28)	0.31	Nasal, REF Paranasal, 0.85 (0.34 to 2.14)	0.73
Residual disease after surgery	R0, REF R1, 1.52 (0.66 to 3.50)	0.33	R0, REF R1, 1.11 (0.51 to 2.44)	0.79
RT	No, REF Yes, 0.60 (0.21 to 1.71)	0.33	No, REF Yes, 0.86 (0.35 to 2.13)	0.75

T category refers to the eighth edition of the TNM.
Significant p value are typed in bold.
Cat., category; REF, reference category; RT, radiation therapy; TNM, tumor, node, metastases.

furthermore, low immunoscore was significantly associated with shorter OS (p=0.004) and PFS (p=0.04) also at multivariable model including relevant clinicopathological information (table 1). These findings provide evidence on the clinical relevance of the immune contexture in SN-MM.

Integrity of the canonical IFNGR/JAK/STAT signaling pathway in SN-MM cell lines

The IFN-γ has a key role in antitumor immune response; however, cancers exhibit heterogeneous response to IFNs.[12] We investigated the integrity of the IFNGR/JAK/STAT signaling pathway in SN-MM cell lines. By flow cytometry analysis, SN-MM cell lines expressed surface IFNGR1/CD119 on the entire cell population (n=4, mean±SD (%) control (CTRL) 99.5±0.38 vs IFN-γ 99.1±1.46; figure 2A and online supplemental table S5). No differences in terms of expression level were observed in all but SN-MM5 cell line on IFN-γ exposure (figure 2B,C). By western blot analysis, JAK2 was regularly expressed in SN-MM cell lines regardless of stimulation, while JAK1 was decreased by IFN-γ in SN-MM1 and SN-MM2 cell lines (figure 2D). Moreover, we could detect significant induction of STAT1, pSTAT1Y701, and IRF1 expression in SN-MM cell lines 48 hours after the IFN-γ stimulation, as compared with unstimulated cells (figure 2E). Moreover, we observed a stable activation of pSTAT1Y701 and IRF1 at different time points on IFN-γ stimulation among different SN-MM cell lines (figure 2F). Based on these findings, we conclude that as a group, SN-MM are responsive to IFN-γ via IFNGR/JAK/STAT signaling pathway.

Proficient transcriptomic and proteomic response to IFN-γ by SN-MM cells

Transcriptional response to IFN-γ treatment has been analyzed in CM cells and was consistent with the activation of IFN-inducible genes modulating the antigen-presenting machinery, T-cell chemokines as well as G1/S and G2/M checkpoints.[31] With the goal to establish the modes of response to IFN-γ by SN-MM cells, we performed bulk RNA-seq analysis of SN-MM cell lines at baseline and after stimulation with IFN-γ for 4 hours. By principal component analysis (PCA), the five SN-MM cell lines clustered regardless of the stimulation with IFN-γ (figure 3A). As previously demonstrated for CM cell lines,[31] SN-MM cell line identity represents the major contributor to gene expression both at baseline and on exposure to IFN-γ (figure 3A and online supplemental figure S2). According to their derivation, SN-MM cell lines express a large set of lineage and differentiation melanocytic antigens, including PRAME, SOX10, EDNRB, MITF, PMEL, TYR, and MLANA (online supplemental figure S3); their expression remained stable on IFN-γ stimulation (online supplemental figure S4). In addition, we analyzed the gene expression of cancer-testis antigens among cancer cell lines (online supplemental figure S5). Overall, we found heterogeneous expression of cancer-testis antigens among cell lines (online supplemental figures S5 and S6). Moreover, similar to CM, SN-MM cell lines express PRAME, MAGE-A, MAGE-B, MAGE-C, NY-ESO-1 (ie, CTAG1A, CTAG1B), and CSAG, some of them being tested in clinical trials for cancer vaccines.[32] A relevant number of genes were significantly modulated (padj<0.05 and LFC >1) by IFN-γ as compared

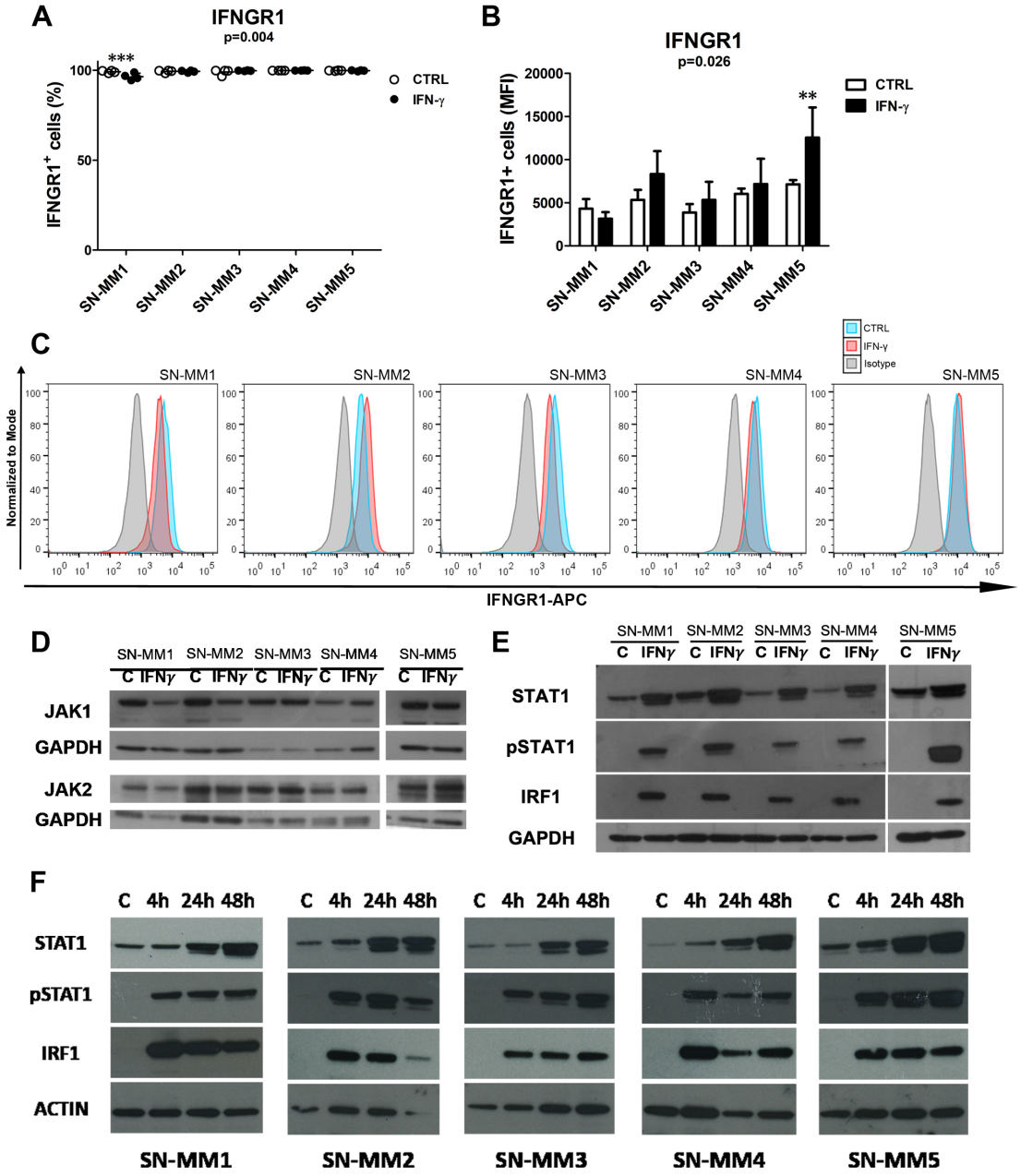

Figure 2 IFNGR/JAK/STAT signaling activation in SN-MM cell lines. (A–C) IFNGR1/CD119 surface expression was analyzed by flow cytometry. The percentages and MFI of IFNGR1-positive cells in SN-MM cell lines are shown at baseline and on IFN-γ treatment (A–B; n=4). Graph's bars represent the mean and SD of biological replicates. Two-way ANOVA statistical analysis and Bonferroni's multiple comparison post-test have been performed; **p<0.01; ***p<0.001. Representative histogram plots showing IFNGR1 expression (MFI) at baseline (turquoise) and on IFN-γ treatment (red) in each SN-MM cell line are shown (C). Gray histograms represent isotype controls. (D–F) Representative western blots showing activation of IFN-γ signaling pathway in SN-MM cell lines. JAK1 and JAK2 expression is shown in unstimulated (C) or IFN-γ stimulated samples after 48 hours (D; n=3). pSTAT1(Tyr701), STAT1, and IRF1 expression are shown in unstimulated or IFN-γ stimulated samples for 48 hours after o/n starvation with 1% FBS (E; n=3) and over time after IFN-γ stimulation (F); GAPDH or ACTIN were used as housekeeping control, as labeled. The samples derive from parallel experiments and blots were processed in parallel. ANOVA, analysis of variance; IFN, interferon; IFNGR, IFN-γ receptor; MFI, median of fluorescence intensity; SN-MM, sino-nasal melanoma.

with the unstimulated counterpart (figure 3B), of which 82 upregulated genes were in common between the cell lines (online supplemental table S6), including CD274, CXCL9, CXCL10, CXCL11, IDO1, STAT1, STAT2, STAT3, IRF1, IRF9, TAP1, TAP2, PSMB8, PSMB9, SOCS1, SOCS3, NLRC5, and B2M. Functional enrichment analysis based on GO was highly concordant across cell lines and showed that differentially expressed genes were enriched in relevant biological processes like response to IFNs, regulation of type I IFN production, regulation of IkB kinase/NF-kB signaling, response to virus and apoptotic signaling pathway on IFN-γ treatment (online supplemental figure S7). GSEA, conducted in parallel, corroborated these findings and showed

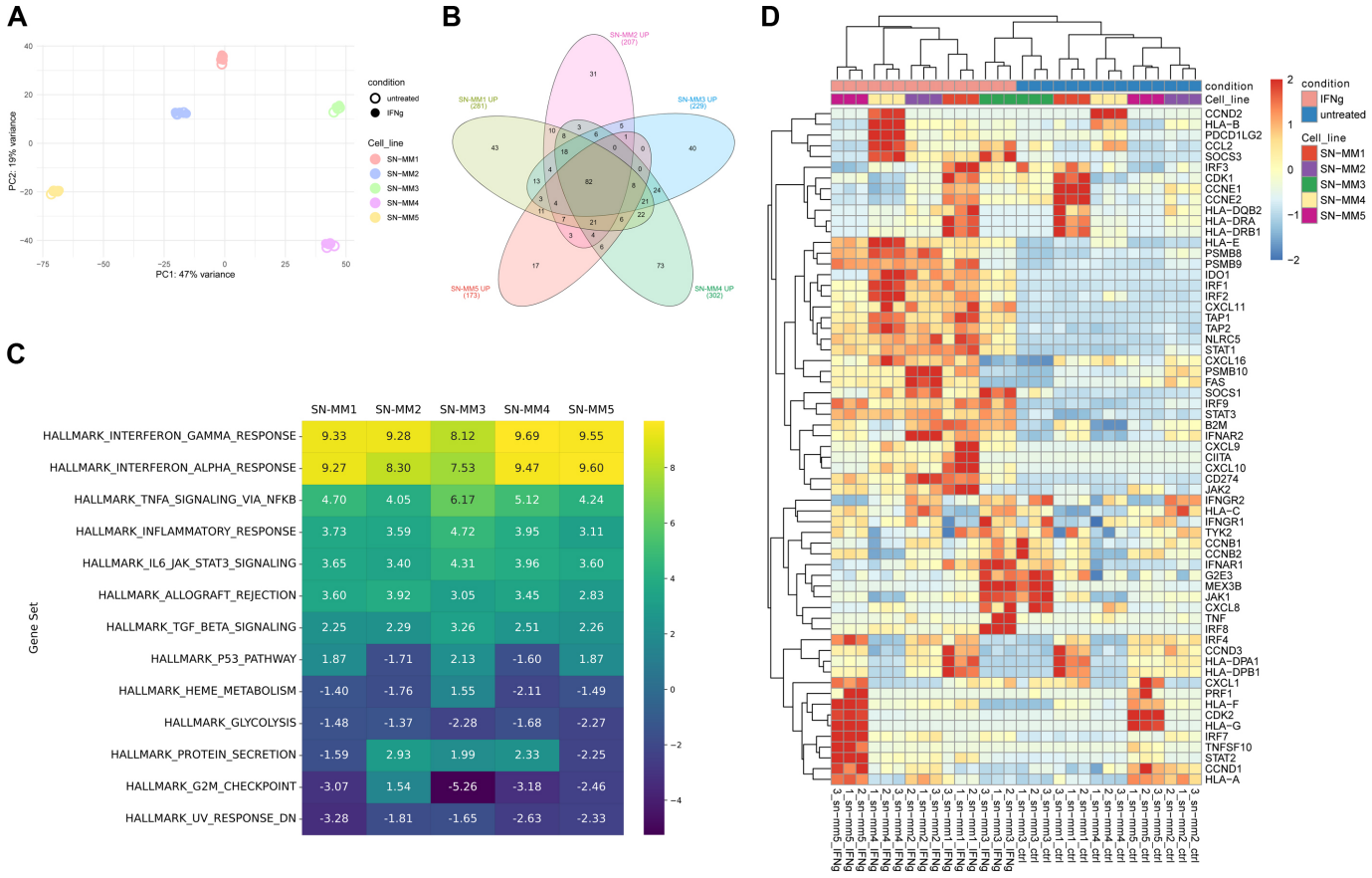

Figure 3 IFN-γ transcriptional response in SN-MM cell lines. (A) Scatter plots showing the combined projections of the first two components of a PCA run considering the expression of the 500 most-variable genes of the SN-MM cell lines untreated or treated with IFN-γ for 4 hours. Samples' features are highlighted by color code. (B) Venn diagram showing the number of common and private upregulated genes in IFN-γ stimulated versus untreated SN-MM cell lines. (C) Heatmap showing the NES values and related q values of HALLMARK gene sets significantly enriched in SN-MM cell lines on IFN-γ treatment, as identified by GSEA. GSEA results were filtered by FDR <0.25. A heatmap has been generated with the seaborn package (Python). (D) Heatmap of unsupervised hierarchical clustering of 63 key IFN-γ response genes expression based on z-scores of normalized expression values (Rlog). IFN, interferon; FDR, false discovery rate; GSEA, Gene Set Enrichment Analysis; NES, normalized enrichment score; PCA, principal component analysis; SN-MM, sino-nasal melanoma.

positive enrichment of IFN response, cytokine signaling, STAT signaling, inflammatory response, allograft rejection, and apoptosis gene sets (figure 3C, online supplemental figure S8 and online supplemental table S7). In parallel, negative enrichment of Glycolysis, UV Response, and G2M checkpoints was observed on IFN-γ treatment (online supplemental table S7). Moreover, significant enrichment of protein secretion, mitotic spindle, MYC targets, E2F targets, and p53 pathway was observed among different cell lines (online supplemental table S7). These findings are highly consistent with published data from IFN-γ treated human cell lines.[31] Finally, we focused on key IFN-γ response genes previously published by Grasso *et al*[31] and performed unsupervised clustering analysis showing a segregation of IFN-γ treated samples versus untreated samples (figure 3D). Overall, RNA-seq data demonstrated an active transcriptional response to IFN-γ, with multiple pathways and IFN-dependent genes modulated on IFN-γ stimulation in all MM cell lines modulating their immunogenicity and cell fitness.

To extend these findings to the post-transcriptional level, we analyzed the proteome of SN-MM cell lines, at baseline and stimulated with IFN-γ (4 hours, 24 hours and 48 hours), by using a mass spectrometry-based untargeted approach. Summarized data at 48 hours showed the strongest response to IFN-γ consistent across all the cell lines. By PCA projections of the proteomic data set, SN-MM1, SN-MM2 and SN-MM5 cell lines segregated along PC1 or PC2 axes according to IFN-γ stimulated or unstimulated conditions, whereas SN-MM3 and SN-MM4 samples clustered along the PCA axes regardless of the stimulation (online supplemental figure S9A). Moreover, all SN-MM cell lines segregated along the PC7 axis according to condition (ie, IFN-γ vs control; online supplemental figure S10), indicating that IFN-γ stimulation drove the protein expression profile, although it was not the major contributor. Furthermore, unsupervised k-means clustering analysis identified five clusters of highly expressed proteins (online supplemental figure S9B) mostly corresponding to unique SN-MM cell lines, regardless of

treatment condition (ie, IFN-γ and CTRL; online supplemental figure S9C), supporting that cell line identity represents the major contributor to protein expression both at baseline and on exposure to IFN-γ. Upstream regulators analysis based on IPA on SN-MM samples stimulated with IFN-γ compared with unstimulated controls corroborated the involvement of IFN-γ (z-score: SN-MM1 2.6; SN-MM2 2.3; SN-MM3 3.2; SN-MM4 2.6; SN-MM5 3.7; online supplemental figure S9D) and STAT1 (z-score: SN-MM1 2.5; SN-MM2 2.9; SN-MM3 2.5; SN-MM4 2.3; SN-MM5 3.6; online supplemental figure S11) as activated upstream regulators. In detail, IFN-γ activated STAT1/2 and stimulated the expression of IFN-inducible proteins (eg, ISG15, IFIT3, IFITM1, IFI16), MHC molecules (eg, HLA-A, HLA-B, HLA-C, HLA-DR), transporters responsible for MHC peptide loading (eg, TAP1 and TAPBP), proteasome subunits (eg, PSME1, PSME2, PSMB10), and immunosuppressive molecule IDO1 (online supplemental figures S9D and S11). The proteomic landscape of IFN-γ-stimulated SN-MM cell lines substantiated the transcriptomic data and demonstrated IFN-γ response at the post-transcriptional level. In conclusion, as a group, based on transcriptomic and proteomic profile, SN-MM cell lines resulted proficient in IFN-γ response.

Survival and immunogenicity features of SN-MM cells are modulated by IFN-γ

IFN-γ exposure can also promote tumor cell apoptosis or cell cycle blockade.[13] Since transcriptomic analysis on SN-MM indicated that G2/M checkpoints are among IFN-γ-induced genes, we tested the effect of IFN-γ treatment on cell viability and proliferation of SN-MM cell lines. By using Annexin V/SYTOX AADvanced flow cytometry assay, the frequency of dead cells was significantly increased after IFN-γ treatment in SN-MM1, SN-MM2 and SN-MM5 cell lines, whereas the viability of SN-MM3 and SN-MM4 was unchanged (p<0.0001, n=4; figure 4A and online supplemental table S5). Particularly, we found a significant increase in Annexin V^+/SYTOX $AADvanced^-$ early apoptotic cells (p<0.0001, n=4; figure 4B and online supplemental table S5) to the disadvantage of Annexin V^+/SYTOX $AADvanced^+$ late apoptotic or necrotic cells (p<0.0001, n=4; figure 4C and online supplemental table S5). Moreover, IFN-γ significantly reduced the proliferation of SN-MM1, SN-MM2, and SN-MM5 cell lines over time (p<0.0001; n=4 mean ± SD (%) 24 hours vs 48 hours vs 72 hours: SN-MM1 89.2±5.2 vs 47.6±9.1 vs 27±1.1; SN-MM2 97±2.5 vs 67.7±3.2 vs 49.9±4.7; SN-MM3 96.7±4.1 vs 109.1±14.5 vs 93.5±5.7; SN-MM4 104.3±2.4 vs 108.3±8.1 vs 102.1±1; SN-MM5 87.6±2.9 vs 64.1±1.9 vs 46.5±4.4; figure 4D). Accordingly, the cell counts relative to unstimulated samples, as measured by MTS assay, were significantly lower in these cell lines, over time (48 hours vs 24 hours; 72 hours vs 48 hours; 72 hours vs 24 hours; figure 4D). In summary, IFN-γ exerted a significant cytotoxic and anti-proliferative effect on three out of five SN-MM cell lines.

Moreover, IFN-γ can modulate tumor immunogenicity by inducing the MHC class I and II antigen-presenting molecules by tumor cells. Thus, we tested the expression of MHC-I (ie, HLA-ABC) and MHC-II (ie, HLA-DR) on SN-MM cell surface by flow cytometry. All SN-MM cell lines showed a consistent fraction expressing MHC-I at the baseline (n=6, mean±SD (%) 95.12±2.65; figure 4E and online supplemental table S5). Moreover, IFN-γ induced a significant upregulation of MHC-I expression (MFI) in four out of five SN-MM cell lines (p<0.0001, n=6; figure 4F, online supplemental figure S12 and online supplemental table S5). On the contrary, MHC-II was variably expressed among SN-MM cell lines. Specifically, we observed a high frequency of $HLA\text{-}DR^+$ cells in three out of five cell lines at baseline (SN-MM1; SN-MM2; SN-MM4), suggesting they might be direct targets of cytotoxic $CD4^+$ T cells.[33] A statistically significant increase of $HLA\text{-}DR^+$ cells was induced by IFN-γ in the remaining cell fraction (p=0.0001, n=3; figure 4G and online supplemental table S5). SN-MM3 and SN-MM5 showed lower expression of HLA-DR both at baseline and on exposure to IFN-γ (figure 4G,H) that could be partially explained by lower CIITA expression[34] in these cell lines (figure 3D). Moreover, HLA-DR expression (MFI) was significantly upregulated by IFN-γ in SN-MM4 (p=0.02, n=3; figure 4H and online supplemental table S5). Hence, SN-MM cell lines were proficient in antigen presentation and were able to upregulate MHC molecules on IFN-γ.

Cancer immune contexture is modulated by paracrine responses of cancer cells and myeloid cells to a set of pro-inflammatory cytokines, resulting in chemokine secretion (ie, CXCL-9, CXCL-10, and CXCL-11), mainly regulated by IFNs.[35] Accordingly, the CXCL-10 production was significantly induced by IFN-γ in SN-MM1, SN-MM2, and SN-MM5 cell lines, whereas no CXCL-10 production was measured in SN-MM3 and SN-MM4 supernatants (p=0.004, n=5; figure 4I and online supplemental table S5).

In conclusion, although all SN-MM cell lines retain an intact antigen-presentation machinery in terms of MHC molecules expression, SN-MM3 and SN-MM4 display a blunted response to IFN-γ in relevant function regulating cancer immunity.

Modulation of IFN-γ-induced PD-L1 protein expression in SN-MM

IFN-γ signaling represents the master regulator of the expression of the PD-L1 and PD-L2 inhibitory receptors in different cell types, including CM cells.[16] Cancer cell expression of PD-L1 guides escape from immune surveillance by binding to PD-1 on T cells leading to their apoptosis, anergy and functional exhaustion. This adaptive immune resistance mechanism is overcome by anti-PD-1/PD-L1 therapy. Notably, PD-L1 was highly expressed on cell surfaces on exposure to IFN-γ in SN-MM1, SN-MM2, and SN-MM5 cell lines; on the contrary, SN-MM3 and SN-MM4 cell lines expressed significantly lower levels of this molecule (p<0.0001, n=4; figure 5A,B and online

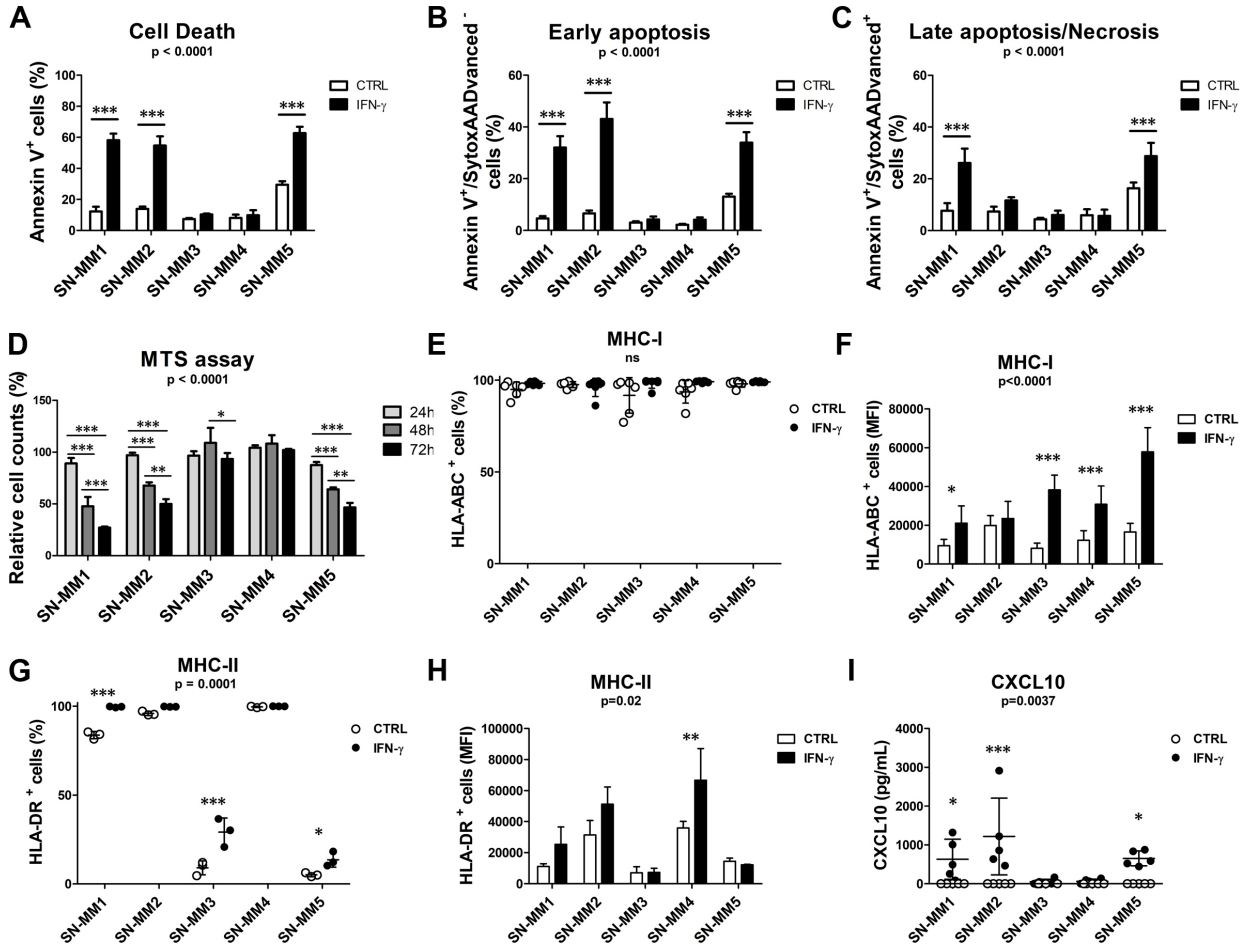

Figure 4 IFN-γ functional response among SN-MM cell lines. SN-MM cell lines were treated with IFN-γ or unstimulated (CTRL) to evaluate cytotoxic and anti-proliferative effect (A–D), MHC molecules (E–H) and CXCL10 production (I). (A–C) After 72 hours, the cell viability was analyzed with Annexin V/SYTOX AADvanced staining by flow cytometry. Column bar graphs illustrate the percentage of dead (Annexin V$^+$; A), early apoptotic (Annexin V$^+$/V/SYTOX AADvanced$^-$; B) and late apoptotic or necrotic (Annexin V$^+$/V/SYTOX AADvanced$^+$; C) cells (n=4). (D) Viability and proliferation of SN-MM cell lines treated with IFN-γ were measured by MTS assay. Column bar graph represents the percentage of viable cells, after administration of IFN-γ (100 U/mL) for 24 hours, 48 hours, and 72 hours relative to untreated SN-MM cells (n=3). (E–I) After 48 hours, HLA-ABC (E, F) and HLA-DR (G, H) surface expression were analyzed by flow cytometry. Scatter plots illustrate the percentage of positive cells (E, G) and column bar graphs illustrate the MFI (F, H) (n=4). (I) CXCL-10 production was measured by ELISA on SN-MM cell lines supernatants obtained after 48 hours of culture. Graph's bars represent the mean and SD of biological replicates. Two-way ANOVA statistical analysis and Bonferroni's multiple comparison post-test have been performed. *p<0.05; **p<0.01; ***p<0.001. ANOVA, analysis of variance; CTLR, control; HLA-ABC, Human Leukocyte Antigens ABC; HLA-DR, Human Leukocyte Antigens DR; IFN, interferon; MFI, median of fluorescence intensity; MHC, major histocompatibility complex; MTS, 3-(4,5-dimethylthiazol-2-yl)-5-(3-carboxymethoxyphenyl)-2-(4-sulfophenyl)-2H-tetrazolium, inner salt; SN-MM, sino-nasal melanoma.

supplemental figure S12). This finding was further validated on sections from cell block preparation of cell lines using IHC and by western blot (figure 5C,D). The modulation of PD-L1 protein expression at different time points after IFN-γ stimulation was unchanged among SN-MM cell line (figure 5E); specifically, we could detect PD-L1 expression 14 hours after IFN-γ stimulation that was stable until 72 hours post-stimulation, whereas we could not detect PD-L1 at earlier time points (ie, 4 hours; figure 5A). Overall, heterogeneity among SN-MM cell lines also affects PD-L1 expression. The blunted responses observed in SN-MM3 and SN-MM4 could not be explained by transcriptional modulation, as observed by many other IFN-γ-inducible transcripts (figure 3), nor by different expression kinetics of the receptor activation (figure 2). Moreover, as for many other IFN-γ-inducible genes, we could not detect loss-of-function mutations in PD-L1/CD274 by RNA-seq (online supplemental tables S8–S12). Of note, SN-MM3 and SN-MM4 express significantly lower levels of many relevant melanocytic markers (ie, MITF, PMEL, MLANA, TYR, TYRP1, TYRP2, S100B) and other melanoma antigens (ie, SLC45A2 and EDNRB) (online supplemental figures S3 and S4).

Overall, these findings support the hypothesis that PD-L1 regulation in SN-MM relies on molecular mechanisms beyond canonical IFN-γ signaling, potentially linked to cell-intrinsic differentiation programs.

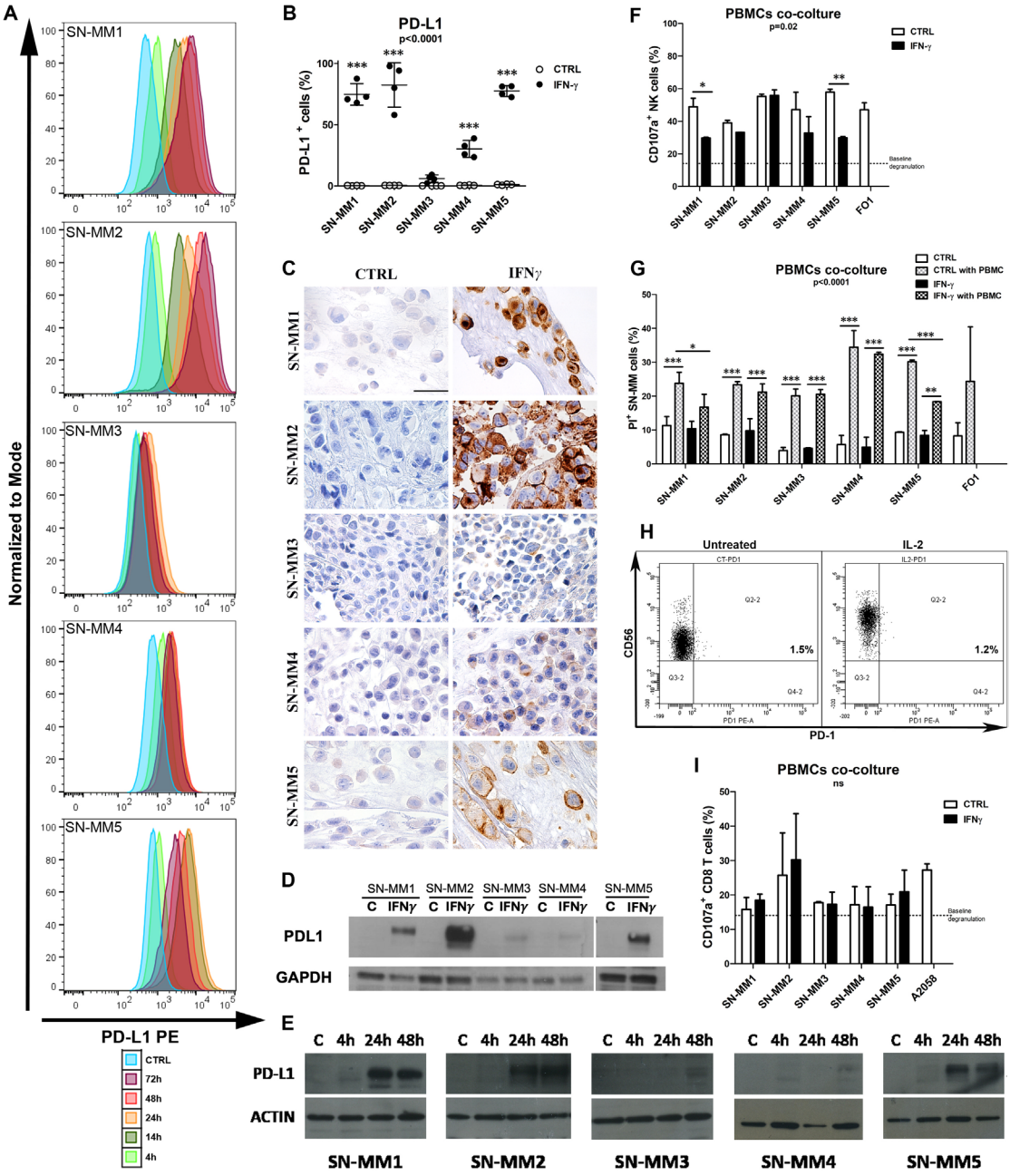

Figure 5 PD-L1 expression among SN-MM cell lines. (A–B) PD-L1 surface expression was evaluated by flow cytometry on five SN-MM cell lines. Representative histogram plots showing PD-L1 expression (MFI) at baseline (CTRL) and on IFN-γ treatment at different time points, as labeled (A). A scatter plot illustrates the percentage of PD-L1 positive cells after 48 hours of IFN-γ stimulation (B; n=4). Graphs bars represent the mean and SD of biological replicates. Two-way ANOVA statistical analysis and Bonferroni's multiple comparison post-test have been performed; ***p<0.001. (C) IHC for PD-L1 on cell blocks from SN-MM cell lines. Sections are counterstained with hematoxylin. Magnification 40×; scale bar 50 µm. (D–E) Western blots showing PD-L1 expression in SN-MM cell lines unstimulated (C) or stimulated with IFN-γ for 48 hours (D) or over time (E), as labeled; GAPDH or ACTIN were used as housekeeping control. The samples derive from parallel experiments and blots were processed in parallel. (F–I) SN-MM cell lines were treated o/n with IFN-γ or unstimulated (CTRL) and co-cultured with activated PBMCs isolated from healthy donors at a 1:3 (F–G) or 1:1 (I) effector-to-target ratio. FO1 and A2058 CM cell lines were used as controls. (F, I) The CD107a expression is evaluated on $CD56^+$ NK cells (F; n=2) and $CD8^+$ T cells (I; n=3) by flow cytometry after co-culture with target tumor cells. Dashed lines indicate the percentage of $CD107a^+$ cells cultured without target cells. The target tumor cells viability was assessed with PI staining by flow cytometry (G). A column bar graph illustrates the percentage of dead tumor cells after culture with or w/o activated PBMCs. Graph bars represent the mean and SD of biological replicates. Two-way ANOVA statistical analysis and Bonferroni's multiple comparison post-test have been performed; *p<0.05; **p<0.01; ***p<0.001. (H) Representative dot plots showing PD-1 expression by flow cytometry on NK cells untreated or stimulated with IL-2. ANOVA, analysis of variance; CM, cutaneous melanomas; CTRL, control; IFN, interferon; IL, interleukin; MFI, median of fluorescence intensity; NK, natural killer; PBMC, peripheral blood mononuclear cell; PD-1, programmed cell death protein-1; PD-L1, programmed cell death ligand 1; SN-MM, sino-nasal melanoma.

Susceptibility of SN-MM cell to NK-cell killing

NK cells can recognize and eliminate malignant cells without prior antigen sensitization and do not rely on peptide-MHC complexes for target cell recognition, but their function is finely regulated by the engagement of activating and inhibitory receptors defining their cytotoxic potential.[36] Specifically, tumor cells that downregulate MHC class I or express stress-induced ligands become susceptible to NK cell-mediated killing. However, engineered NK cells that target tumor antigens or overcome tumor evasion mechanisms could be developed for cancer immunotherapy.[37 38]

In this study, SN-MM cells were treated with IFN-γ o/n or untreated and incubated with allogeneic PBMCs to evaluate the susceptibility of SN-MM to effector cells. Specifically, we tested degranulation and cytotoxic activity of NK cells and $CD8^+$ T cells from co-cultures by performing a CD107a degranulation assay and evaluating tumor cell viability by propidium iodide staining. HLA-I masking on tumor cells has been performed to avoid the engagement of the MHC class I–specific inhibitory receptors, such as the killer cell immunoglobulin-like receptors.[36] First, we observed the upregulation of degranulation marker expression by $CD56^+$ NK cells on co-culture with tumor cells as compared with PBMCs alone (figure 5F). Moreover, SN-MM cells increased the percentage of $CD107a^+$ NK cells (mean range: 39%–57.7%) similarly to the cutaneous melanoma cell line FO1 (mean: 47%; figure 5F), suggesting that SN-MM cells trigger the NK cell effector function. To further expand this finding, we evaluated tumor cell viability on co-culture with activated PBMCs (figure 5G). Allogeneic NK cells kill approximately 20–35% of target cells after 5 hours of co-culture (figure 5G). However, IFN-γ significantly impaired the ability of SN-MM1 and SN-MM5 cell lines to induce NK cell degranulation (figure 5F); accordingly, the percentage of cell death was significantly reduced in IFN-γ-treated versus untreated SN-MM1 and SN-MM5 cell lines on co-culture with activated PBMCs (figure 5G). By programmed cell death protein-1 (PD-1) staining on NK cells (figure 5H), we have excluded the interaction between the PD-1 inhibitory receptor and the IFN-γ-induced PD-L1 on SN-MM cell surface.

We subsequently tested CTL. The frequency of $CD107a^+$ CTL was not substantially increased on co-culture with tumor cells, as compared with PBMCs alone, in all but SN-MM2 and A2058 (figure 5I), suggesting a limited CTL degranulation and induced killing of SN-MM cells. Moreover, the IFN-γ treatment of SN-MM cells before co-culturing with PBMCs did not significantly affect $CD8^+$ T cells degranulation (figure 5I). Altogether, these in vitro findings support susceptibility of SN-MM cells to NK cell-mediated killing; however, IFN-γ can promote tumor cell escape mechanisms from effector NK cells,[39] whose mechanisms remain to be defined.

Identification of personalized neoantigen candidates in SN-MM

By integrated analysis of whole-exome sequencing and RNA-seq data using the pVAC-Seq pipeline, we have defined the neoantigen landscape of SN-MM cell lines. Class I and class II HLA haplotypes were inferred directly from tumor sequencing data using an ensemble of established tools (as described in online supplemental M&M), revealing high heterozygosity across HLA loci, a molecular feature supporting broad neoantigen presentation potential (online supplemental tables S3). By somatic variant calling we have identified nonsynonymous SNVs and InDels,[40] which were subsequently annotated for amino acid changes and evaluated for transcript and variant allele expression (online supplemental tables S13–S22). Across the five SN-MM cell lines, we could identify between 258 and 416 candidate neoantigens per cell line, of which between 46 and 82 met stringent "Pass-tier" criteria, including strong predicted binding and presentation, clonal tumor allele frequency, and detectable variant allele expression (figure 6A, online supplemental figure S13A,B and online supplemental tables S13–S22). The contribution of individual expressed HLA alleles to the high-confidence class I neoantigen repertoire varied markedly across cell line, highlighting allele-specific differences in predicted immunogenicity (online supplemental figure S13C); however, we observed strong neoantigen predictions for most HLA alleles. Both class I and class II analyses yielded a substantial number of high-confidence candidates (figure 6B).

By analyzing the TCGA (The Cancer Genome Atlas) cutaneous melanoma cohort, we revealed that the number of protein-altering variants expressed at the RNA level is comparable between SN-MM and CM (figure 6C), suggesting that these tumors could be equally targeted by neoantigen vaccine therapies.[41] Finally, we predicted high-quality neoantigen candidates for each SN-MM, incorporating binding affinity, presentation probability, and allele expression (figure 6D–H). Of note, some of these high-quality neoantigens correspond to SN-MM mutations in known oncogenes, including SOX10, ABLIM3, RB1, CDK12, PTEN, ANKRD11, KLF4, NOTCH2, RAF1, TP53, FAT1, IRS2, MAP3K14, MCL1, ZFHX3.

Collectively, these findings demonstrate that SN-MM harbor a rich repertoire of expressed, high-quality neoantigens, supporting the view that MM is a potentially immunogenic tumor type and providing a foundation for selecting candidate targets for T cell-based immunotherapy development.

DISCUSSION

IFN-γ is a pleiotropic cytokine exerting key tumor suppressor functions.[12 21 35] Resistance to IFN-γ is mediated by different mechanisms including innate immune resistance that leads to T-cell dysfunction, although this can be bypassed with ICI.[22 28] ICIs have significantly improved outcomes for patients with previously untreatable cancers,

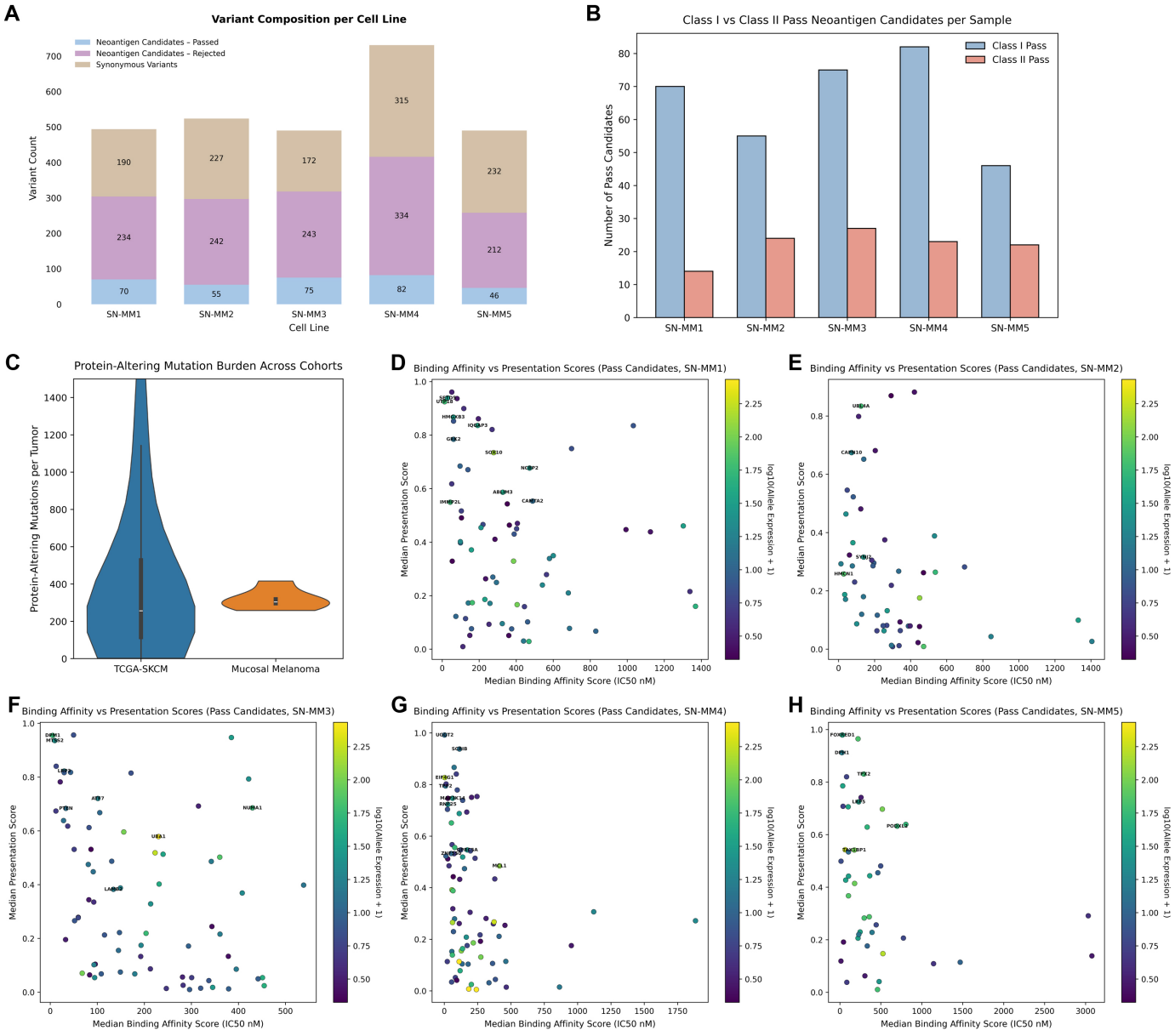

Figure 6 Tumor-specific neoantigens prediction in SN-MM. (A) The bar graph corresponds to the total counts of variants per cell line, showing the number of synonymous and non-synonymous variants, the latter including candidate neoantigens that passed or failed filtering criteria. (B) Number of "pass-tier" neoantigen candidates predicted to bind HLA class I and HLA class II molecules. (C) Protein-altering mutation burden in the five SN-MM cell lines compared with CM from TCGA. For the TCGA-SKCM cohort, we used the sample designations from cBioPortal for the TCGA-GDC dataset of 474 tumors. (D–H) Scatter plots showing the relationship between the predicted binding affinity (x-axis) and presentation probability (y-axis) for Pass-tier neoantigen candidates in each SN-MM cell line; each point represents one candidate, colored by allele expression level. Lower binding affinity score indicates stronger peptide–MHC binding. A higher presentation score indicates higher peptide processing, transport, and binding stability. Prioritization of top neoantigen candidates is illustrated by gene name labeling. CM, cutaneous melanomas; GDC, Genomic Data Commons; HLA, human leukocyte antigen; MHC, major histocompatibility complex; SKCM, skin cutaneous melanoma; SN-MM, sino-nasal melanoma; TCGA, The Cancer Genome Atlas.

particularly those that express PD-L1 and exhibit high immunogenicity, as evidenced by T-cell infiltration and IFN-γ sensitivity.[28] However, these features are still underexplored in MM. By using microscopy on clinical samples, most SN-MM are immune desert and largely devoid of CTLs, a feature predicting unfavorable outcomes, with a subgroup enriched in immunosuppressive TREM2$^+$ TAMs. Despite the limited immune infiltration, the neoantigen prediction analysis reveals a substantial repertoire of tumor neoantigens, supported by broad HLA heterozygosity and expression of melanocytic and cancer-testis antigens, suggesting that SN-MM are not intrinsically refractory to immune recognition. By functional omics approaches on a unique set of SN-MM cell lines,[23] most but not all SN-MM cell lines are intrinsically responsive to IFN-γ. Proficient IFN-γ response in most SN-MM

cell lines exerts antitumor functions leading to increased cell recognition pathways and reduced tumor cell survival and proliferation. These findings suggest that a combination of immune escape mechanisms might occur in MM tissue involving IFN-γ availability and sensitivity by tumor cells along with dysfunction of other checkpoints of the cancer immunity cycle leading to immune exclusion.[28 42] These checkpoints represent the foundation for a proper patient selection to immunotherapeutic strategies. Unfavorable immunoscore with reduced T-cell infiltration predicted poor outcomes in patients with SN-MM, as well documented in most cancer types.[30] Although underpowered in terms of sample size, this set of preliminary findings might suggest trajectories for large-scale multicenter studies in this rare form of melanoma, since SN-MM lacks reliable independent clinical prognosticators.[43 44] Different mechanisms drive the T-cell exclusion (TCE) in cancers to elude immune surveillance. These include low levels of cancer cell immunogenicity, defects in antigen presentation and T-cell priming by antigen-presenting cells, impaired T-cell trafficking to the tumor site, or suppression of T cells by tumor microenvironment (TME).[28 45] Unexpectedly, results from this study propose a rich repertoire of expressed neoantigens in SN-MM that could elicit effective T-cell responses, validating the immunogenicity of these tumors. Cancer cell-intrinsic molecular abnormalities play a key role in driving the TCE.[46 47] This has been observed also in CMs,[46] including gain of function (WNT-β catenin, MYC) and loss of function (LKB1, PTEN, p53) mutations. These abnormalities eventually result in the modulation of T cell-attracting chemokines or recruitment of immunosuppressive myeloid cells promoting TCE.[47] Previously published data showed PTEN loss in SN-MM[23] associated with activation of the PI3K-Akt-mTOR pathway[23 48 49]; we speculate that PI3K-Akt-mTOR blockade might synergize with ICI also in a subgroup of SN-MM, as already found in other cancer types.[50 51] TCE is also mediated by cancer cells being unresponsive or hyporesponsive to IFN-γ.[21 35] We observed a blunted response to IFN-γ in SN-MM3 and SN-MM4 cell lines, but the canonical IFN-γ receptor signaling is preserved at both transcriptional and proteomic levels. Genetic and epigenetic abnormalities in members of the IFN-γ pathway are responsible for primary or acquired hypo-responsiveness to IFN-γ, as well documented for CMs.[22] No mutation has been detected in the IFN-γ pathway and IFN-inducible genes in these two cell lines, highlighting a novel molecular mechanism that requires further investigation. Based on previous data[23] and further refined in this study, SN-MM3 and SN-MM4 dedifferentiation, as measured by low expression of MA, might contribute to a blunted IFN-γ response. This observation requires confirmation at the molecular level, to further include MA expression as static biomarkers for the initial screening of IFN-γ refractoriness of melanocytic tumors.[52] It should be noted that MITF represents the master regulator of melanocyte differentiation from neural crest cells and of the expression of pigmentation-related genes, but also proliferation, apoptosis, invasiveness and metastasis formation in melanoma. Its expression is finely regulated by upstream activators and suppressors operating on transcriptional, post-transcriptional and post-translational levels, also including epigenetic and microenvironmental signals.[52] Dedifferentiation into a mesenchymal phenotype impacts the activity of T cells and pro-inflammatory pathways affecting the immunotherapy efficacy.[52] The genetic or epigenetic rescue of MITF might guide MM differentiation and likely cooperate with immunotherapeutic strategies. However, mechanistic interactions between the MITF network and immunotherapy resistance, beyond the involvement of pigmentation-related antigens, remain undetermined.[53] Functional assays further revealed that SN-MM cells are susceptible to NK-cell-mediated killing, although IFN-γ exposure can promote tumor cell escape mechanisms from effector NK cells.[39]

Overall, the scenario of MM as proposed by this study is highly heterogeneous and consistent with a potentially immunogenic tumor type. Indeed, we proposed that immune exclusion mechanisms, rather than lack of antigenic targets, limit responsiveness to current immunotherapies. It should be noted that MM variably retain melanoma-associated antigens based on transcript and protein expression ([23]and this study). Moreover, a set of cancer-testis antigens is expressed in SN-MM cell lines, some of them already tested in clinical trial vaccines.[32] Finally, we provide a set of personalized neoantigen candidates that could be targeted by T cell-based immunotherapy or cancer vaccines.[54] For MM showing unresponsiveness to IFN-γ by transformed cells, immunotherapeutic approaches should be tailored on the tumor-specific genetic or epigenetic basis of the defect. On the contrary, most MM displaying sensitivity to IFN-γ might significantly benefit from strategies increasing the local availability of IFN-γ in combination with ICI. This group might profit from exogenous administration of IFN-γ or direct IFN-γ delivery through CAR T-cell therapies. Alternatively, indirect IFN-γ inducing strategies might be considered, such as administration of pattern recognition receptor agonists in the form of adjuvants. Newly, epigenetic therapy in combination with ICIs has been demonstrated to increase IFN-γ signature and PD-L1 expression within the TME and reprogram the systemic host immune response.[26] We acknowledge that, despite capturing variable degrees of differentiation and immunogenicity, patient-derived SN-MM cell lines cannot fully recapitulate the extensive genetic and biological heterogeneity observed in patients with MM in clinical settings.

Understanding the intrinsic cancer immune biology and its dysfunctional step is crucial to adapt therapies to the various cancer immune phenotypes. To this end, the integration of static biomarkers exploring the immune genome and the TME of cancer with functional assay might significantly improve our ability to allocate patients with MM to various immunotherapeutic options. Along

this line is the development of the recently emerged functional precision oncology field.[27]

Author affiliations
[1]Molecular and Translational Medicine, Università degli Studi di Brescia, Brescia, Italy
[2]Unit of Pathology, ASST Spedali Civili di Brescia, Brescia, Italy
[3]Department of Neuroscience, University of Padua, Padua, Italy
[4]Unit of Otorhinolaryngology – Head and Neck Surgery, Azienda Ospedale Universita Padova, Padua, Italy
[5]Department of Biotechnology, University of Verona, Verona, Italy
[6]Department of Transfusion Medicine, ASST Spedali Civili di Brescia, Brescia, Italy
[7]Department of Otorhinolaryngology, Head and Neck Surgery, Maastricht University Medical Centre+, Maastricht, The Netherlands
[8]National Center for Gene Therapy and Drugs based on RNA Technology - CN3, Padova, Italy
[9]Consorzio Interuniversitario per le Biotecnologie (CIB), Trieste, Italy
[10]Department of Translational Medicine, University of Eastern Piedmont Amedeo Avogadro School of Medicine, Novara, Italy
[11]Center for Autoimmune and Allergic Diseases, University of Eastern Piedmont Amedeo Avogadro School of Medicine, Novara, Italy
[12]Department of Sciences and Technological Innovation, University of Eastern Piedmont Amedeo Avogadro - Alessandria Campus, Alessandria, Italy
[13]Unit of Otorhinolaryngology and Head and Neck Surgery, University of Insubria Department of Biotechnology and Life Sciences, Varese, Italy
[14]Unit of Oncology, ASST Spedali Civili di Brescia, Brescia, Italy
[15]Department of Medical and Surgical Specialties, Università degli Studi di Brescia, Brescia, Italy
[16]Medicine, Washington University School of Medicine in Saint Louis, St. Louis, Missouri, USA
[17]Washington University in St Louis School of Medicine, St Louis, Missouri, USA
[18]Pathology and Immunology, Washington University School of Medicine in Saint Louis, St. Louis, Missouri, USA

Acknowledgements We would like to thank the pathologists, technicians, clinicians, nurses, and administrative employees who have provided support to the study and the follow-up of patients with cancer.

Contributors MMo: Conceptualization, Investigation, Visualization, Methodology, Writing-original draft, Project administration. SP: Investigation, Visualization. AB: Investigation, Methodology. MF: Formal analysis, Investigation, Visualization, Writing-original draft. MB: Investigation, Visualization. IP: Investigation. MC: Investigation. GC: Investigation. MO: Formal analysis. GL: Data curation. LBG: Methodology. FM: Formal analysis. GF: Investigation. VB: Investigation. SR: Investigation. GT: Investigation. SP: Resources, Investigation. MMa: Resources, Data curation, Funding acquisition, Investigation. VDG: Data curation, Investigation. EM: Resources. MT-Z: Resources. PN: Resources. FC: Resources. DL: Resources, Formal analysis. PM: Formal analysis, Visualization. MR: Resources, Supervision. JL: Formal analysis, Visualization. OG: Resources, Supervision. MG: Investigation, Formal analysis, Resources, Supervision. WV: Conceptualization, Resources, Supervision, Funding acquisition, Writing-original draft, Project administration. WV is the guarantor.

Funding This work was financially supported by the Associazione Italiana per la Ricerca sul Cancro (Italian Association for Cancer Research) (AIRC IG-23179), AIRC 5 × 1000 grant n. 22757, "Valentino Morbio" Fondazione Spedali Civili Brescia, and SARAP Onlus (Brescia). MMo was supported by Fondazione Umberto Veronesi. SR was supported by Fondazione Umberto Veronesi and Fondazione Cariplo (Grant ID: 2021-1563).

Competing interests None declared.

Patient consent for publication Not applicable.

Ethics approval The studies involving human participants were reviewed and approved by the Institutional Ethics Board of ASST Spedali Civili of Brescia (IRB code: NP 2066/2015) and ASST Sette Laghi of Varese (IRB code: NP 33025/2015), Italy. Participants gave informed consent to participate in the study before taking part.

Provenance and peer review Not commissioned; externally peer reviewed.

Data availability statement All data relevant to the study are included in the article or uploaded as supplementary information. All data relevant to the study are included in this published article or uploaded as supplemental information files. The RNA-sequencing data generated and analyzed in this study are publicly available in Gene Expression Omnibus (GEO) (https://www.ncbi.nlm.nih.gov/geo/; RRID:SCR_005012) under accession number GSE287519. The protein-coding genes expression data analyzed in this study were obtained from Depmap portal (DepMap Public 24Q4, https://depmap.org/portal/data_page/?tab=currentRelease) for DepMap cell lines (https://doi.org/10.25452/figshare.plus.27993248.v1). The mass spectrometry proteomics data generated in this study are publicly available in ProteomeXchange Consortium via the PRIDE partner repository with the dataset identifier PXD059186. The WES data analyzed in this study have been submitted to NCBI (https://www.ncbi.nlm.nih.gov/sra), under accession number PRJNA1356825. For revision purposes, reviewers may access data at the following link: https://dataview.ncbi.nlm.nih.gov/object/PRJNA1356825?reviewer=kbj6ac5v61oev6v8n4bff4tlnu.

ORCID iD
William Vermi https://orcid.org/0000-0002-2291-2997

REFERENCES

1 Curti BD, Faries MB. Recent Advances in the Treatment of Melanoma. *N Engl J Med* 2021;384:2229–40.
2 Klemen ND, Wang M, Rubinstein JC, *et al*. Survival after checkpoint inhibitors for metastatic acral, mucosal and uveal melanoma. *J Immunother Cancer* 2020;8:e000341.
3 Teterycz P, Czarnecka AM, Indini A, *et al*. Multimodal Treatment of Advanced Mucosal Melanoma in the Era of Modern Immunotherapy. *Cancers (Basel)* 2020;12:3131.
4 Ascierto PA, Accorona R, Botti G, *et al*. Mucosal melanoma of the head and neck. *Crit Rev Oncol Hematol* 2017;112:136–52.
5 Amit M, Na'ara S, Hanna EY. Contemporary Treatment Approaches to Sinonasal Mucosal Melanoma. *Curr Oncol Rep* 2018;20:10.
6 Amit M, Tam S, Abdelmeguid AS, *et al*. Mutation status among patients with sinonasal mucosal melanoma and its impact on survival. *Br J Cancer* 2017;116:1564–71.
7 Hayward NK, Wilmott JS, Waddell N, *et al*. Whole-genome landscapes of major melanoma subtypes. *Nature New Biol* 2017;545:175–80.
8 Moya-Plana A, Herrera Gómez RG, Rossoni C, *et al*. Evaluation of the efficacy of immunotherapy for non-resectable mucosal melanoma. *Cancer Immunol Immunother* 2019;68:1171–8.
9 Klebaner D, Saddawi-Konefka R, Finegersh A, *et al*. Immunotherapy in sinonasal melanoma: treatment patterns and outcomes compared to cutaneous melanoma. *Int Forum Allergy Rhinol* 2020;10:1087–95.
10 Samstein RM, Lee C-H, Shoushtari AN, *et al*. Tumor mutational load predicts survival after immunotherapy across multiple cancer types. *Nat Genet* 2019;51:202–6.
11 Nakamura Y, Zhenjie Z, Oya K, *et al*. Poor Lymphocyte Infiltration to Primary Tumors in Acral Lentiginous Melanoma and Mucosal Melanoma Compared to Cutaneous Melanoma. *Front Oncol* 2020;10.
12 Dunn GP, Koebel CM, Schreiber RD. Interferons, immunity and cancer immunoediting. *Nat Rev Immunol* 2006;6:836–48.
13 Kaplan DH, Shankaran V, Dighe AS, *et al*. Demonstration of an interferon γ-dependent tumor surveillance system in immunocompetent mice. *Proc Natl Acad Sci USA* 1998;95:7556–61.
14 Han J, Wu M, Liu Z. Dysregulation in IFN-γ signaling and response: the barricade to tumor immunotherapy. *Front Immunol* 2023;14.
15 Farrar MA, Schreiber RD. The molecular cell biology of interferon-gamma and its receptor. *Annu Rev Immunol* 1993;11:571–611.

16 Garcia-Diaz A, Shin DS, Moreno BH, *et al*. Interferon Receptor Signaling Pathways Regulating PD-L1 and PD-L2 Expression. *Cell Rep* 2017;19:1189–201.
17 Wang XB, Zheng CY, Giscombe R, *et al*. Regulation of surface and intracellular expression of CTLA-4 on human peripheral T cells. *Scand J Immunol* 2001;54:453–8.
18 Jürgens B, Hainz U, Fuchs D, *et al*. Interferon-γ–triggered indoleamine 2,3-dioxygenase competence in human monocyte-derived dendritic cells induces regulatory activity in allogeneic T cells. *Blood* 2009;114:3235–43.
19 Respa A, Bukur J, Ferrone S, *et al*. Association of IFN-gamma signal transduction defects with impaired HLA class I antigen processing in melanoma cell lines. *Clin Cancer Res* 2011;17:2668–78.
20 Rodig SJ, Gusenleitner D, Jackson DG, *et al*. MHC proteins confer differential sensitivity to CTLA-4 and PD-1 blockade in untreated metastatic melanoma. *Sci Transl Med* 2018;10:eaar3342.
21 Alspach E, Lussier DM, Schreiber RD. Interferon γ and Its Important Roles in Promoting and Inhibiting Spontaneous and Therapeutic Cancer Immunity. *Cold Spring Harb Perspect Biol* 2019;11:a028480.
22 Sucker A, Zhao F, Pieper N, *et al*. Acquired IFNγ resistance impairs anti-tumor immunity and gives rise to T-cell-resistant melanoma lesions. *Nat Commun* 2017;8:15440.
23 Monti M, Benerini Gatta L, Bugatti M, *et al*. Novel cellular systems unveil mucosal melanoma initiating cells and a role for PI3K/Akt/mTOR pathway in mucosal melanoma fitness. *J Transl Med* 2024;22:35.
24 Edge SB, Compton CC. The American Joint Committee on Cancer: the 7th edition of the AJCC cancer staging manual and the future of TNM. *Ann Surg Oncol* 2010;17:1471–4.
25 Vescovi R, Monti M, Moratto D, *et al*. Collapse of the Plasmacytoid Dendritic Cell Compartment in Advanced Cutaneous Melanomas by Components of the Tumor Cell Secretome. *Cancer Immunol Res* 2019;7:12–28.
26 Qin T, Mattox AK, Campbell JS, *et al*. Epigenetic therapy sensitizes anti-PD-1 refractory head and neck cancers to immunotherapy rechallenge. *J Clin Invest* 2025;135:e181671.
27 Letai A, Bhola P, Welm AL. Functional precision oncology: Testing tumors with drugs to identify vulnerabilities and novel combinations. *Cancer Cell* 2022;40:26–35.
28 Chen DS, Mellman I. Elements of cancer immunity and the cancer–immune set point. *Nature New Biol* 2017;541:321–30.
29 Bugatti M, Bergamini M, Missale F, *et al*. A Population of TIM4+FOLR2+ Macrophages Localized in Tertiary Lymphoid Structures Correlates to an Active Immune Infiltrate Across Several Cancer Types. *Cancer Immunol Res* 2022;10:1340–53.
30 Fridman WH, Zitvogel L, Sautès–Fridman C, *et al*. The immune contexture in cancer prognosis and treatment. *Nat Rev Clin Oncol* 2017;14:717–34.
31 Grasso CS, Tsoi J, Onyshchenko M, *et al*. Conserved Interferon-γ Signaling Drives Clinical Response to Immune Checkpoint Blockade Therapy in Melanoma. *Cancer Cell* 2021;39:122.
32 Nin DS, Deng L-W. Biology of Cancer-Testis Antigens and Their Therapeutic Implications in Cancer. *Cells* 2023;12:926.
33 Axelrod ML, Cook RS, Johnson DB, *et al*. Biological Consequences of MHC-II Expression by Tumor Cells in Cancer. *Clin Cancer Res* 2019;25:2392–402.
34 Steimle V, Siegrist CA, Mottet A, *et al*. Regulation of MHC class II expression by interferon-gamma mediated by the transactivator gene CIITA. *Science* 1994;265:106–9.
35 Gocher AM, Workman CJ, Vignali DAA. Interferon-γ: teammate or opponent in the tumour microenvironment? *Nat Rev Immunol* 2022;22:158–72.
36 Vivier E, Tomasello E, Baratin M, *et al*. Functions of natural killer cells. *Nat Immunol* 2008;9:503–10.
37 Biederstädt A, Rezvani K. Engineered natural killer cells for cancer therapy. *Cancer Cell* 2025;43:1987–2013.
38 Burón M, Etxebarria A, Álvarez M, *et al*. Natural killer cells in adoptive cell therapy: current landscape of genetic engineering strategies. *Oncoimmunology* 2025;14:2563099.
39 Liu X. The paradoxical role of IFN-γ in cancer: Balancing immune activation and immune evasion. *Pathology - Research and Practice* 2025;272:156046.
40 Monti M, Romanello MB, Agnelli L, *et al*. Genomic profiling of mucosal melanoma identifies novel fusion transcripts and therapeutic molecular hubs. *SSRN* [Preprint] 2025.
41 Zhang X, Goedegebuure SP, Chen MY, *et al*. Neoantigen DNA vaccines are safe, feasible, and induce neoantigen-specific immune responses in triple-negative breast cancer patients. *Genome Med* 2024;16:131.
42 Gajewski TF. The Next Hurdle in Cancer Immunotherapy: Overcoming the Non-T-Cell-Inflamed Tumor Microenvironment. *Semin Oncol* 2015;42:663–71.
43 Lechner M, Takahashi Y, Turri-Zanoni M, *et al*. International Multicenter Study of Clinical Outcomes of Sinonasal Melanoma Shows Survival Benefit for Patients Treated with Immune Checkpoint Inhibitors and Potential Improvements to the Current TNM Staging System. *J Neurol Surg B Skull Base* 2023;84:307–19.
44 Ferrari M, Mattavelli D, Tomasoni M, *et al*. The MUSES⁎: a prognostic study on 1360 patients with sinonasal cancer undergoing endoscopic surgery-based treatment. *Eur J Cancer* 2022;171:161–82.
45 Spranger S. Mechanisms of tumor escape in the context of the T-cell-inflamed and the non-T-cell-inflamed tumor microenvironment. *Int Immunol* 2016;28:383–91.
46 Wellenstein MD, de Visser KE. Cancer-Cell-Intrinsic Mechanisms Shaping the Tumor Immune Landscape. *Immunity* 2018;48:399–416.
47 Spranger S, Gajewski TF. Impact of oncogenic pathways on evasion of antitumour immune responses. *Nat Rev Cancer* 2018;18:139–47.
48 Turri–Zanoni M, Medicina D, Lombardi D, *et al*. Sinonasal mucosal melanoma: Molecular profile and therapeutic implications from a series of 32 cases. *Head Neck* 2013;35:1066–77.
49 Jurmeister P, Wrede N, Hoffmann I, *et al*. Mucosal melanomas of different anatomic sites share a common global. *J Pathol* 2022;256:61–70.
50 Zhang Z, Richmond A, Yan C. Immunomodulatory Properties of PI3K/AKT/mTOR and MAPK/MEK/ERK Inhibition Augment Response to Immune Checkpoint Blockade in Melanoma and Triple-Negative Breast Cancer. *IJMS* 2022;23:7353.
51 Wispelaere W, Annibali D, Tuyaerts S, *et al*. PI3K/mTOR inhibition induces tumour microenvironment remodelling and sensitises p^{S6}. *Clin Transl Med* 2024;14.
52 Massi D, Mihic-Probst D, Schadendorf D, *et al*. Dedifferentiated melanomas: Morpho-phenotypic profile, genetic reprogramming and clinical implications. *Cancer Treat Rev* 2020;88:102060.
53 Bai X, Fisher DE, Flaherty KT. Cell-state dynamics and therapeutic resistance in melanoma from the perspective of MITF and IFNγ pathways. *Nat Rev Clin Oncol* 2019;16:549–62.
54 Ohta S, Misawa A, Kyi-Tha-Thu C, *et al*. Melanoma antigens recognized by T cells and their use for immunotherapy. *Exp Dermatol* 2023;32:297–305.